Publications of the Astronomical Society of the Pacific, **123**:341–347, 2011 March

A Coronagraph Using a Liquid Crystal Array and a Deformable Mirror for Active Apodizing and Phase Corrections

Deqing Ren,[1,2,3] and Yongtian Zhu[1,2]

Received 2010 October 5; accepted 2011 January 11; published 2011 February 23

ABSTRACT. Almost all high-contrast imaging coronagraphs proposed until now are based on passive coronagraph optical components. That is, the coronagraph cannot be actively controlled to be optimized for best performance. Pupil apodizing, which modifies the light transmission on the pupil, is one of the promising techniques for high-contrast imaging. Here, we propose, for the first time, a high-contrast imaging coronagraph that integrates a liquid crystal array for active pupil apodizing and a deformable mirror for active phase correction. In such a way, source errors such as the initial transmission error and wavefront error can be actively and efficiently compensated based on an optimized algorithm, which is optimized for maximum contrast in the discovery area. In addition, the use of a liquid crystal array makes this system more flexible and able to create any apodizing pupil, including square or circle aperture with or without central obstruction. In this article, we discuss the working principle and estimated performance of the coronagraph. We also demonstrate that the chromatic aberration induced by a liquid crystal array is sufficiently small, which makes it suitable to be used for ground-based near-infrared coronagraphic Extreme-AO systems.

Online material: color figures

1. INTRODUCTION

Since the discovery of a planet around 51Peg (Mayor & Queloz 1995), the number of known exoplanets around solar type stars has increased to more than 400 today. These exoplanets have been discovered mostly using the indirect detection based on the radial velocity measurement. Given the current methods, the majority of exoplanets discovered so far have minimum masses that are typical of giant gaseous planets and orbit radii of, at most, a few astronomical units (Stam et al. 2004; Butter et al. 2006). Apart from some orbital and mass parameters, little is known about exoplanets' physical characteristics, such as the atmosphere conditions and chemical compositions. The characterization of an exoplanet's atmosphere requires the direct detection of photons from the exoplanet.

Direct detections of exoplanets remain challenging, since exoplanets are very faint. A high-contrast coronagraph is needed to suppress the star diffraction light, so that the local exoplanet can be detected. For a direct detection of an Earth-like planet, a contrast of 10^{-9}–10^{-10} is required in the visible, and it is generally agreed that such detection can be done only with a space telescope because of the unavoidable optical wavefront error induced by the atmosphere. However, recent theoretical simulations (Marley et al. 2007; Wuchterl 2000) and observations (Marois et al. 2008; Serabyn et al. 2010) confirmed that for young and Jupiter-like exoplanets, a contrast in the order of only 10^{-5} is needed in the infrared around the 1.25–5.0 wavelength range.

Many high-contrast imaging coronagraphs have been proposed recently (see the review by Guyon et al. 2006). Among them is the transmission apodization coronagraph (Nisenson and Papaliolios 2001; Aime et al. 2002; Gonsalves and Nisenson 2003). Traditional transmission apodization coronagraphs use a fixed transmission function to modulate the light transmission on the pupil, and high-contrast imaging can be achieved in theory. A problem for such an apodization coronagraph is the difficulty of manufacturing the apodization pupil, since the transmission needs to be controlled at every spatial position on the pupil with a high degree of precision that cannot be changed after manufacturing. The binary apodization mask (Vanderbei et al. 2004) mitigates some manufacturing issues, but is not able to actively control amplitude in an actual coronagraph operation.

The active correction of amplitude for high-contrast imaging has been proved to be more challenging, and no simple solution has been found until now. Two deformable mirrors (DMs) were proposed for the correction of intensity variation induced by the atmospheric turbulence (Roggemann and Lee 1998; Lee 2006), but this approach can only provide a correction in a small magnitude range, with the goal of providing a uniform intensity that is induced by the atmospheric turbulence, and is not suitable for

[1] National Astronomical Observatories/Nanjing Institute of Astronomical Optics & Technology, Chinese Academy of Sciences, Nanjing 210042, China.

[2] Key Laboratory of Astronomical Optics & Technology, Nanjing Institute of Astronomical Optics & Technology, Chinese Academy of Sciences, Nanjing 210042, China.

[3] Physics & Astronomy Department, California State University Northridge, 18111 Nordhoff Street, Northridge, CA 91330–8268; ren.deqing@csun.edu.

the coronagraph pupil apodizing, where large transmission differences ranging from 0%–100% are involved. Furthermore, the 2-DM approach is more complex and no real operation has been reported. In his early work, Angel (1994) pointed out that such scintillation effect must be corrected adaptively if planets are to be detected efficiently. The need for amplitude correction with high-contrast imaging where a contrast of 10^{-7} or better is required was confirmed by the simulation (Stahl & Sandler 1995) and further confirmed by recent laboratory testing (Biller et al. 2009) in which a DM is used to create a dark hole and it was found that the high-contrast discovery area will be reduced significantly by the amplitude error.

In this article, we propose, for the first time, a high-contrast imaging coronagraph that integrates a liquid crystal array (LCA) and a DM for active pupil apodizing and phase corrections, respectively. The LCA will not only provide the required pupil apodizing, it will also be able to perform active amplitude correction. In such an approach, source errors such as the initial transmission error and wavefront error can be actively compensated based on an optimized algorithm, which is optimized for the maximum contrast in the discovery area. In addition, the use of a LCA makes such a system more flexible and able to create any apodizing pupil, including square or circle apertures with or without central obstruction, which can make the coronagraph work with any telescope. Since the coronagraph is based on linear polarized light, two identical coronagraphs can be deployed to make 100% use of the incoming light. In § 2, we discuss the general principle of the active coronagraph. In § 3, we simulate the coronagraph performance for wideband imaging. We present our conclusions in the last section.

2. THEORY OF THE LIQUID CRYSTAL CORONAGRAPH

2.1 Liquid Crystal Coronagraph

Our coronagraph deploys a LCA and a DM. The LCA is used to modulate the light transmission pattern, and the DM is used to correct possible wavefront error. The SLM that we used is an array of twisted nematic liquid crystals. The schematic diagram of the active coronagraph is shown in Figure 1. Our coronagraph consists of a collimator, a polarizer (polarizer 1), a LCA, an analyzer (polarizer 2), a DM, and a camera lens. The LCA is sandwiched between polarizers 1 and 2, so that the magnitude of the incoming linear polarized light can be modulated by the LCA. In this figure, for the convenience of description, the LCA is a transmission component, whereas in an actual system we will use a reflective LCA that has many advantages over a transmissive one, such as high filling factor and high white-black contrast. In our coronagraph, the LCA is used to control the transmission, and the DM is used for the phase correction. In such a way, both the pupil transmission and the phase can be controlled in a closed-loop system in an active way until the performance is consistent with the design goal.

In Figure 1, the income beam is split as two parts by polarizer 1. On average, each part takes 50% of the incoming beam. This figure only shows one coronagraph, which makes use of 50% of the telescope light. The other 50% linear polarized light can be used by the second coronagraph. In the visible, an exoplanet only reflects its starlight, and the exoplanet light and the starlight have different polarizations, so the images from the two active coronagraphs can be further used for polarization differential imaging, which has the potential to provide an extra contrast gain. In the infrared, the light from the exoplanet may not be polarized, since thermal radiation is dominant. In this case, images obtained from these two coronagraphs can be simply added.

The general theory of a twisted nematic liquid crystal used as a spatial light modulator (SLM) was discussed by Lu and Saleh (1990). The twisted nematic liquid crystal is an anisotropic medium that can be treated locally as an uniaxial crystal whose optical axis is parallel to the direction of the molecules. The long axis of the molecules defines the direction of the extraordinary index. Because of the twist, the molecules rotate gradually in a helical fashion, which changes the polarization orientation. If the LCA is sandwiched between two polarizers, the light transmitted in each pixel of the array can be adjusted by setting the voltage applied, and the twist angle is a function of the applied voltage. The liquid crystal device used is sandwiched between a polarizer and an analyzer, making angles ψ_1 and ψ_2 with the x axis, which is vertical with the propagation direction of the income wave. Assume that the ordinary and extraordinary indices of the liquid crystal materiel are n_0 and n_e, respectively, and the thickness of the liquid crystal device is d. When $\psi_1 = 90°$ and $\psi_2 = 0°$, the phase variation is small. In such a 90°–0° configuration (i.e., $\psi_1 = 90°$ and $\psi_2 = 0°$), the transmission T and phase δ for a liquid crystal are

$$T = 1 - \left(\frac{\pi}{2\gamma}\right)^2 \sin^2(\gamma), \tag{1}$$

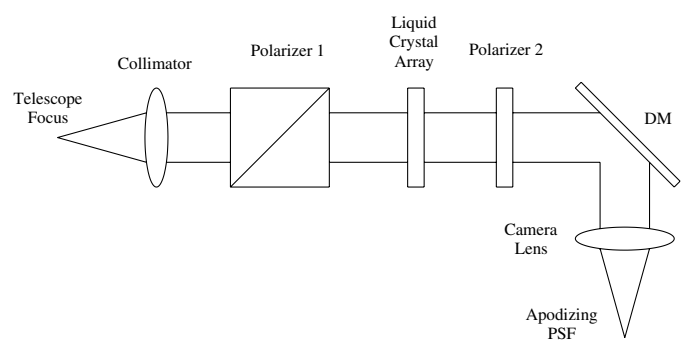

FIG. 1.—Schematic diagram of the liquid crystal apodizing coronagraph. Both the liquid crystal array and the DM can be controlled by a computer for active correction according to an optimization algorithm until best performance is achieved.

$$\delta = \beta - \tan^{-1}\left[\frac{\beta}{\gamma}\tan(\gamma)\right], \tag{2}$$

where

$$\beta = \frac{\pi d}{\lambda}[n_e(\theta) - n_o], \tag{3}$$

$$\gamma = \left[\left(\frac{\pi}{2}\right)^2 + \beta^2\right]^{1/2}. \tag{4}$$

When an electric filed is applied on the liquid crystal, all molecules are assumed to tilt by an angle θ, tending to align with the applied field. The angle θ increases with the applied field until reaching a saturation value of $\pi/2$. As a result of the molecule tilting, the extraordinary index of the refraction can be calculated as

$$\frac{1}{n_e^2(\theta)} = \frac{\cos^2(\theta)}{n_e^2} + \frac{\sin^2(\theta)}{n_o^2}. \tag{5}$$

The transmission T is a monotonic function of β in the interval 0 to 0.866π. Therefore, the value of $\beta = 0.866\pi$ represents the limiting value for the operation of a liquid crystal device as an intensity or transmission modulator. The refractive indices n_e and n_o are typically wavelength-dependent. From equation (3), it is clear that β is also a function of wavelength. A coronagraph using LCA may therefore suffer from the chromatic effect, which will limit the bandwidth for high-contrast imaging.

Figure 2 shows the phase error as a function of β that is relevant with the applied voltage. Although the phase error is small in the 90°–0° configuration, it has a maximum value of 1.2 radians that is still too large for high-contrast imaging. However, such a static wavefront error can be corrected by a DM. The associated intensity/transmission as a function of β is shown in Figure 3. The transmission is not linearly proportional to β (also not linearly proportional to the applied voltage). Therefore, careful calibration of the applied voltages as a function of the transmission is needed.

One concern for the use of LCA is the chromatic aberration for wideband imaging. The refractive indices of the LC material are variable as a function of wavelength and can be calculated by the dispersion formula

$$n = C_1 + C_2\lambda^{-2} + C_3\lambda^{-4}, \tag{6}$$

where C_1, C_2, and C_3 are dispersion constants that characterized the chromatic property of the liquid crystal material.

2.2 Coronagraph Active Correction

The LCA and the DM serve as transmission and phase correctors, respectively. A scientific camera that is located on the coronagraph focal plane is used for the point-spread function (PSF) sensing. The active corrections are based on a numerical optimization algorithm (such as eq. [9]) and is done iteratively until the best performance is achieved.

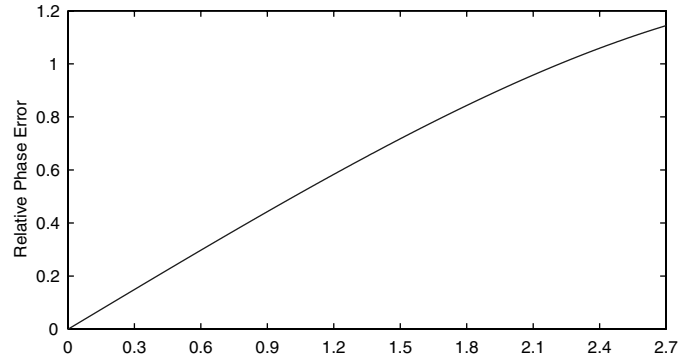

FIG. 2.—Relative phase error (in radians) as a function of β. See the electronic edition of the *PASP* for a color version of this figure.

The LCA and the DM are located on or near the pupil plane. Assume that there are n pixels on the LCA whose transmission can be modulated independently by applied voltages, and there are m actuators on the DM whose strokes can be controlled. The PSF on the focal plane (with rectangular coordinates x and y) is related with the pupil function by a Fourier transfer as

$$I(x,y) = |\vec{F}\{[A_0 \cdot A(v_1, v_2, \ldots, v_n)]e^{-i[\Phi_0 - \Phi(u_1, u_2, \ldots, u_m)]}\}|^2, \tag{7}$$

where $\vec{F}$ represents the operation of the two-dimensional Fourier transform; A_0 and $A(v_1, v_2, \ldots, v_n)$ are the original amplitude and the corrected amplitude, respectively; A_0 is determined by the initial design transmission pattern, and $A(v_1, v_2, \ldots, v_n)$ is associated with an extra compensation that is provided by applying extra voltages $(v_1, v_2, \ldots, v_n)$ on the LCA; Φ_0 is the initial phase error of the coronagraph, including that induced by the LCA, and $\Phi(u_1, u_2, \ldots, u_m)$ is associated with an extra phase compensation by applied voltages $(u_1, u_2, \ldots, u_m)$ on the DM actuators. Both $(v_1, v_2, \ldots, v_n)$ and $(u_1, u_2, \ldots, u_m)$ are free

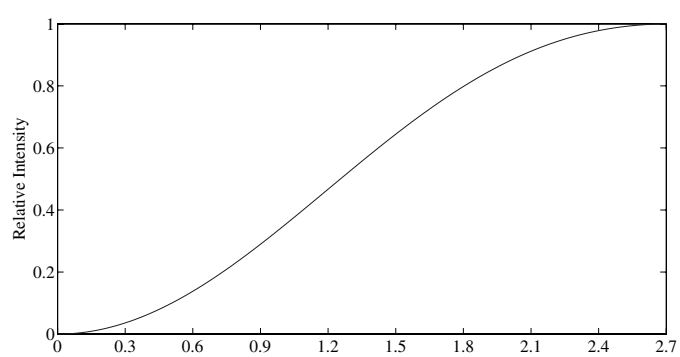

FIG. 3.—Relative transmission/intensity as a function of β. See the electronic edition of the *PASP* for a color version of this figure.

variables that must be optimized via an active iteration until a best performance is achieved.

The contrast is defined as the ratio of intensity on a specific location (x, y coordinates) to the peak intensity on the PSF center (0,0 coordinates) and is given as

$$C(r) \equiv I(x, y)/I(0, 0). \tag{8}$$

The contrast is optimized in the discovery area that is defined by the inner work angular (IWA) distance and the outer work angular (OWA) distance. For such an active correction using both a LCA and a DM, we use the scientific camera located on the focal plane for PSF contrast sensing. Assuming that the target contrast C_t is a constant (such as $10^{-5.5}$ for a ground-based observation), one algorithm that is based on the discrete optimization is to minimize the sum of the intensity in the discovery area:

$$\min\left\{\sum_{\mathrm{IWA}}^{\mathrm{OWA}} |C(r) - C_t|\right\}. \tag{9}$$

Since $(v_1, v_2, \ldots, v_n)$ and $(u_1, u_2, \ldots, u_m)$ are free variables, there are $n + m$ variables that can be optimized. Please note that this algorithm requires the use of a high-dynamic CCD camera (at least 16 bits) to properly sample the PSF in the discovery area.

3. SIMULATION AND DISCUSSIONS

The LCA can be used to create any transmission pattern for a transmission apodization pupil that uses a finite number of transmission elements and is based on a design of discrete optimization (Ren & Zhu 2007). To demonstrate the possible performance of the LCA for high-contrast imaging, we use a LCA to create a transmission pattern for an off-axis telescope without central obstruction, although other transmission patterns that are optimized for circular apertures with central obstruction can also be created with the LCA. Apodization pupils with central obstruction were discussed in our other article (Ren et al. 2010), in which transmission pattern is realized by metallic coating. For the coated filters, the coating of metallic material needs to be controlled with high precision, which is a great challenge. The transmission accuracy is not a problem for the LCA array, however, since the transmission on each pixel can be measured and calibrated in advance. Such an active adjustment guaranties that high precision is achievable.

To demonstrate wideband high-contrast imaging with a finite number of liquid crystals, we use 100 liquid crystal pixels to sample the diameter of the pupil, which yields a moderate time to optimize the design. The intensity of each pixel along the radius can change independently. Because of the symmetry of the transmission pattern, this gives 50 individual variables for the numerical optimization (i.e., $n = 50$). More sampling pixels should generally provide a better result, since more variables are available for the numerical optimization. Figure 4 shows the transmission pattern (*left*) optimized for an off-axis telescope without central obstruction and the associated PSF (*right*). The design is optimized for 10^{-5} high-contrast imaging with a ground-based telescope at a discovery area corresponding to an angular distance from 2–21 λ/D. For ground-based high-contrast imaging, near-infrared observations are preferred, considering the radiation features of the star-planet system and the performance of adaptive optics. The contrast at the 1.25 μm design wavelength is shown in Figure 5, where the dashed line is the PSF without apodizing. In this example, the LCA coronagraph is designed to deliver a contrast of 10^{-5} at an angular distance $\geq 2\ \lambda/D$.

Since the liquid crystal material has strong chromatic features in general and the transmission, as well as the phase, is a function of wavelength, as we have discussed, the contrast will be degraded if the observation wavelength is deviated from the design wavelength. We assume that a DM can only correct the static aberration at the design wavelength. The contrast degradation may result from the deviation of wavefront aberration and the transmission, because of the change of wavelength. The refractive index at different wavelengths is calculated according to equation (6). For this simulation, we choose the liquid crystal material MLC-9200-000, which has an Abbe number $V_e = 42.87$ with the dispersion constants $C_1 = 1.4600$, $C_2 = 0.0058$, and $C_3 = 3.95 \times 10^{-17}$ for the ordinary ray and $C_1 = 1.5382$, $C_2 = 0.0073$, and $C_3 = 4.00 \times 10^{-5}$ for the extraordinary ray. The tilt angle θ is found from equation (5) at the design wavelength and is then used to calculate the transmission and phase at other wavelengths using equations (1) and (2). Figure 6 shows the contrasts at different wavelengths in the J band with the phase error only, and Figure 7 shows the contrasts at different wavelengths with the transmission errors only. The shift of wavelengths from 1.25 μm to 1.15 and 1.35 μm results in a slight contrast degradation at the small angular distance (around 2 λ/D). However, the coronagraph is still able to deliver a contrast of 10^{-5} in the J band at an angular distance larger than 2.5 λ/D. It is obvious that the LCA coronagraph is more sensitive to the transmission error than that of the wavefront. We also used other crystal materials for this simulation and have found that differences for different materials are too small to be noticeable. This is because the performance of liquid crystal for wideband high-contrast imaging is dominated by equation (3), which is a function of wavelength, not by the dispersion formula of equation (6). This simulation demonstrated that the chromatic aberration of LCAs is sufficiently small to allow their use for the ground-based near-infrared wideband imaging at a moderate contrast. Further increasing the contrast will reduce the allowed bandwidth accordingly and requires compensation between the contrast and bandwidth, which should be determined in the design simulation process.

For an actual system of the liquid crystal coronagraph, the PSF sensing for the DM and the transmission corrections can be done in the whole J band. This may result in a performance

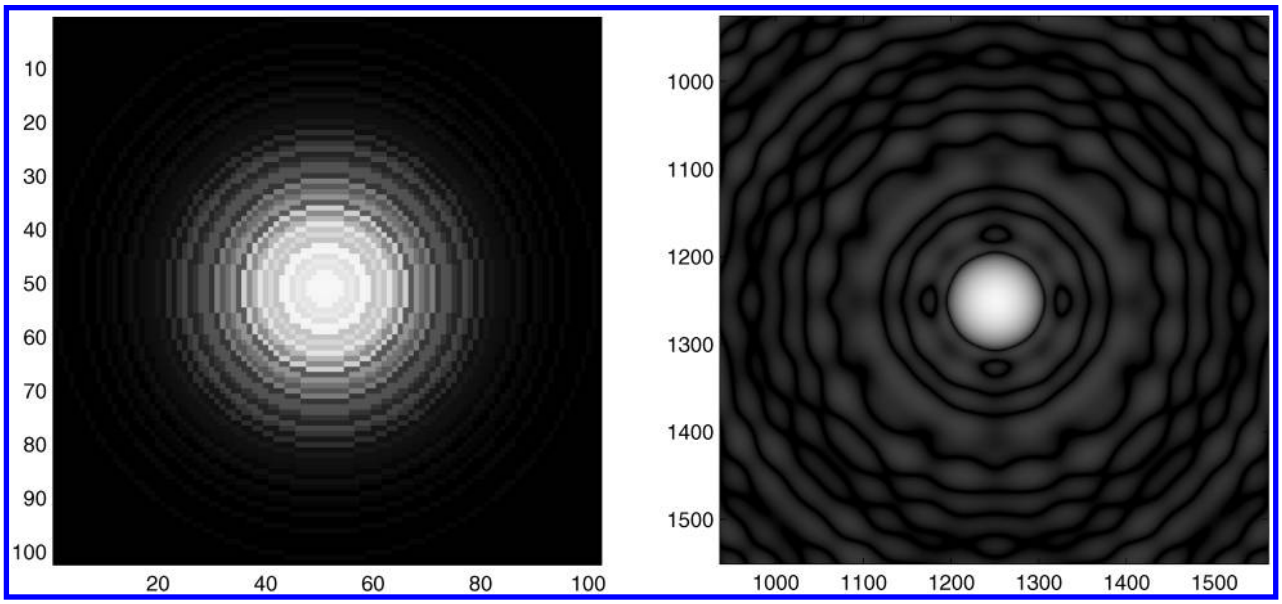

FIG. 4.—Transmission pattern (*left*) and the associated PSF (*right*) created with 100×100 discrete liquid crystal pixels.

that is optimized for the whole J band, instead of for the monochromatic design wavelength as we did in our simulation. Therefore, the overall performance for wideband imaging may be slightly better than in the simulation. The simulation covers almost the whole J band, indicating that the LCA is suitable for ground-based high-contrast imaging.

The LCA has the potential to be used for the transmission apodization coronagraph (Ren & Zhu 2007), which is optimized

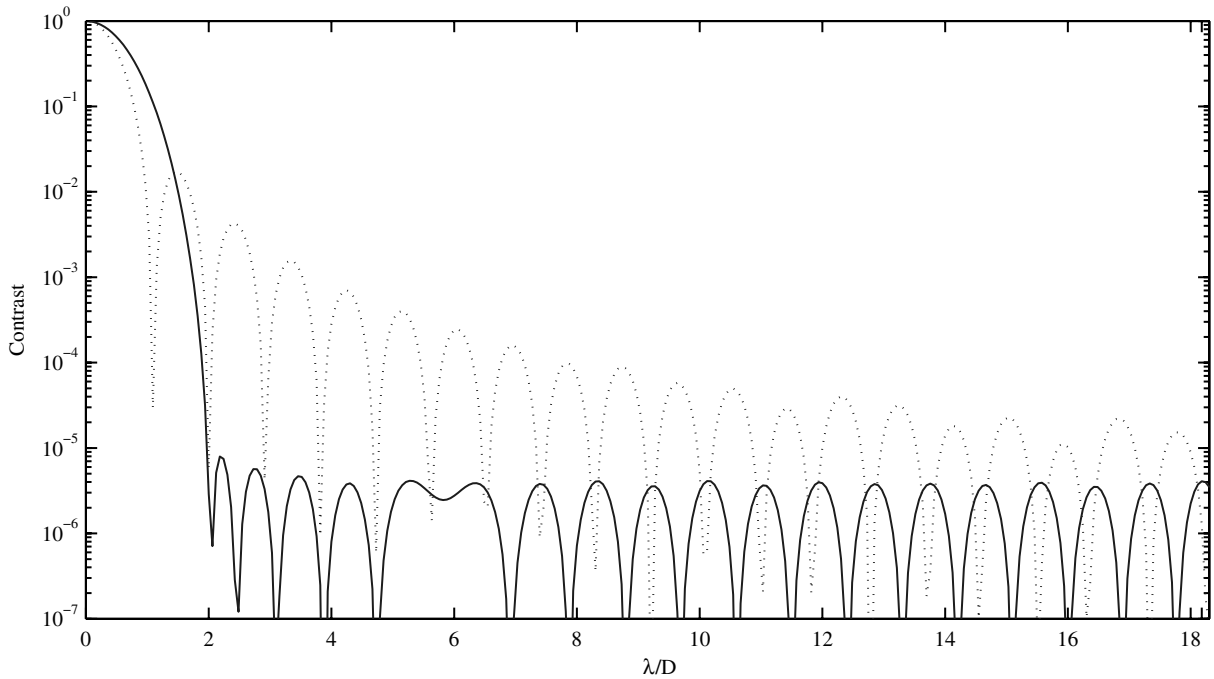

FIG. 5.—Contrast profile for the coronagraph: apodizing pupil (*solid line*) and pupil without apodizing (*dashed line*). The design wavelength is at the 1.25 μm near-infrared. See the electronic edition of the *PASP* for a color version of this figure.

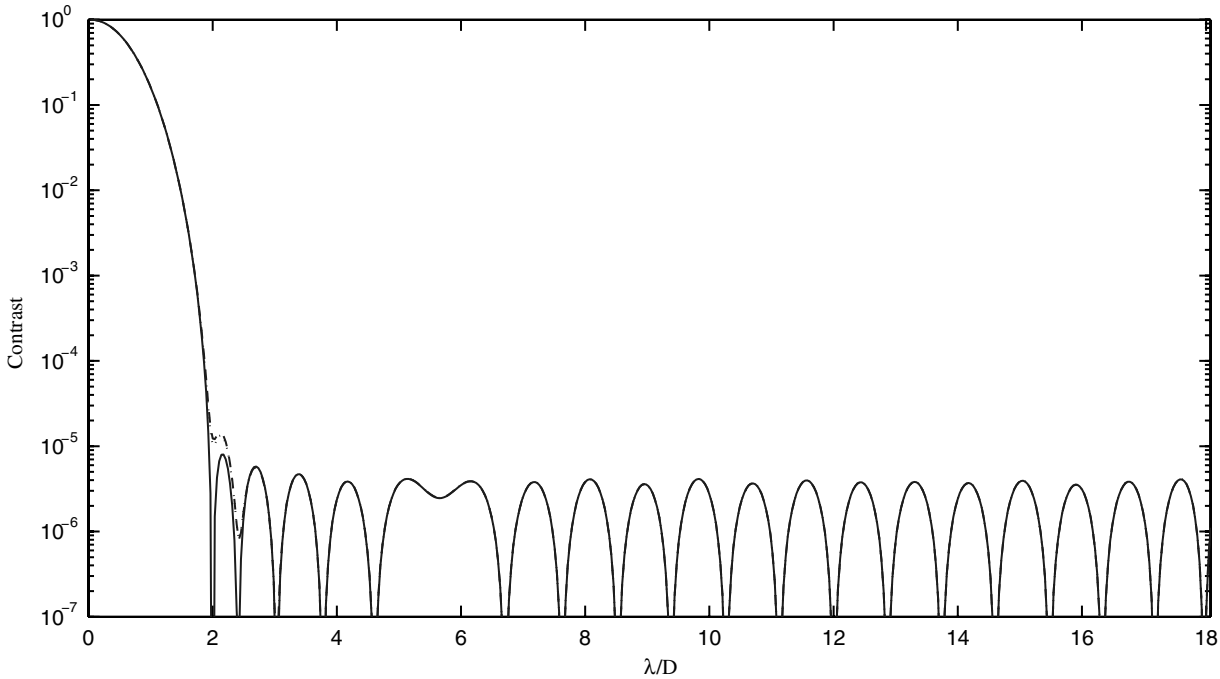

FIG. 6.—Contrasts at different wavelengths when the phase errors are included for wavelengths at 1.25 μm (*solid line*), 1.35 μm (*dotted line*), and 1.15 μm (*dashed line*). See the electronic edition of the *PASP* for a color version of this figure.

for the 10^{-10} contrast with a space-based telescope in the visible. In this case, the LCA must be designed to be achromatic for wideband imaging. For chromatic phase error that is induced by the optical-path difference at different wavelengths, a possible solution is the use of a chromatic correction plate that can be located behind the LCA and will be used to induce an inverse

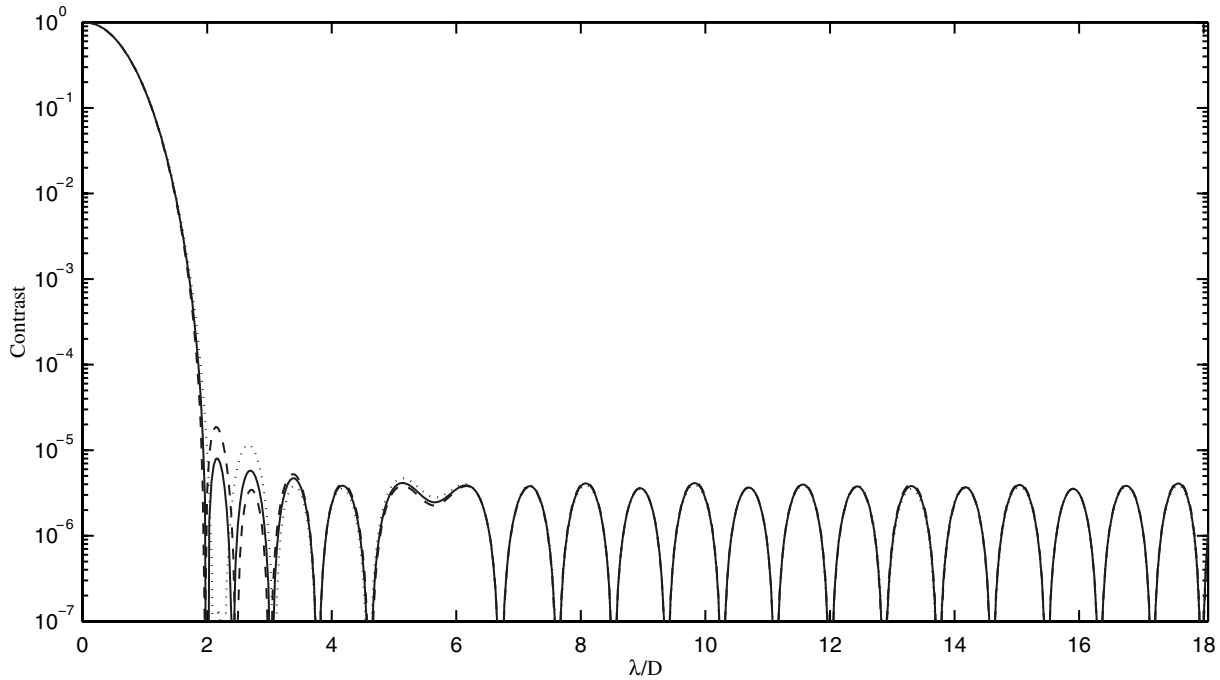

FIG. 7.—Contrasts at different wavelengths when the intensity errors are included for wavelengths at 1.25 μm (*solid line*), 1.35 μm (*dotted line*), and 1.15 μm (*dashed line*). See the electronic edition of the *PASP* for a color version of this figure.

optical-path difference in the collimated rays. In order to induce an inverse optical-path difference, the correction plate can consist of one or more different transmission materials. The general approach to correct the chromatic phase error using different transmission materials was discussed in our previous article (Ren and Allington-Smith 1999). A further fundamental approach to correct the chromatic transmission error is the achromatic correction of β in equation (3). If β is achromatic, both the phase and transmission chromatic errors will be automatically corrected. This can be done by carefully choosing liquid crystal material or by the use of compensation film. At a specific tilt angle θ, β decreases as the wavelength increases. If a liquid crystal material exists for which the $n_e - n_0$ increases properly as the wavelength increases, the chromatic errors will be corrected. For the high-contrast imaging in the visible, the correction of chromatic errors should be further explored.

In the visible, the light from a star is unpolarized, while the starlight reflected by an exoplanet is usually polarized (Seager et al. 2000; Saar and Seager 2003; Hough and Lucas 2003; Stam et al.2004). Polarization measurement can be used to enhance the contrast for the exoplanet imaging. Working in the visible, our coronagraphs can integrate a polarimetry that consists of two coronagraphs, each associated with one of perpendicular linear polarizations that are created by polarizer 1 in figure 1. The two images simultaneously created by the two coronagraphs can be used for wideband differential imaging that has the potential to remove the speckle noise and provide an extra contrast gain on the order of up to 10^{-2} (Zubko et al. 2007) and can therefore further facilitate the high-contrast imaging.

4. CONCLUSIONS

We have, for the first time, proposed a high-contrast imaging coronagraph that integrates a LCA for active transmission correction and a DM for active phase correction. In such an approach, source errors such as the initial transmission and wavefront errors can be actively compensated based on an optimized algorithm. The theory and simulation indicated that a LCA can be used with a DM for wideband imaging with a ground-based telescope in the near-infrared, where a moderate contrast on the order of 10^{-5} is acceptable, without the correction of the chromatic error. Further chromatic correction should be explored if the LCA is used with a space-based telescope in the visible, where a contrast in the order of 10^{-10} is required.

LCAs with pixel numbers over $1\mathrm{K} \times 1\mathrm{K}$ are commercially available at a low price. For example, the LCA Spatial Light Modulator LC-R 1080 manufactured by HOLOEYE has 1920×1200 pixels, with a frame rate of 60 Hz, an intensity ratio of 2000:1, and a 90% fill factor. It works as a reflective component that is based on reflective liquid crystal on silicon. These features make the LCA ideal for the light modulation for the coronagraph pupil apodizing. Laboratory results using LCAs will be discussed in our future articles.

We thank the anonymous referee's helpful comments and corrections, which significantly improved this article. This work was supported by the National Science Foundation (grant ATM-0841440), the National Natural Science Foundation of China (grants 10873024 and 11003031), and the National Astronomical Observatories' Special Fund for Astronomy-2009.

REFERENCES

Aime, C., Soummer, R., & Ferrari, A. 2002, A&A, 389, 334
Angel, J. R. P. 1994, Nature, 368, 203
Biller, B., et al. 2009, PASP, 121, 716
Butler, R. P., et al. 2006, ApJ, 646, 505
Gonsalves, R., & Nisenson, P. 2003, PASP, 115, 706
Guyon, O., Pluzhnik, E. A., Kuchner, M. J., Collins, B., & Ridgway, S. T. 2006, ApJ, 167, 81
Hough, J. H., & Lucas, L. D. 2003, in Towards Other Earths: DARWIN/TPF and Search for Extrasolar Terrestrial Planets, ed. M. Fridlund, & T. Henning (ESA SP-539; Noordwijk: ESA), 11
Lee, L. H., Baker, G. J., & Benson, R. S. 2006, J. Opt. Soc. Am. A, 23, 2602
Lu, Kanghua, & Saleh, Bahaa. E. A. 1990, Opt. Eng., 29, 240
Marley, M. S., et al. 2007, ApJ, 655, 541
Marois, C., et al. 2008, Science, 322, 1348
Mayor, M., & Queloz, D. 1995, Nature, 378, 355
Nisenson, P., & Papaliolios, C. 2001, ApJ, 548, L 201
Ren, D., & Allington-Smith, J. R. 1999, Opt. Eng., 38, 537
Ren, D., Dou, J., & Zhu, Y. 2010, PASP, 122, 590
Ren, D., & Zhu, Y. 2007, PASP, 119, 1063
Roggemann, M. C., & Lee, D. J. 1998, Appl. Opt., 37, 4577
Saar, S. H., & Seager, S. 2003, in ASP Conf. Ser. 294, Scientific Frontiers in Research on Extrasolar Planets, ed.D. Deming, & S. Seager (San Francisco: ASP), 529
Seager, S., Whitney, B. A., & Sasselov, D. D. 2000, ApJ, 540, 504
Serabyn, E., Mawet, D., & Burruss, R. 2010, Nature, 464, 1018
Stahl, S. S., & Sandler, D. G. 1995, ApJL, 454, L153
Stam, D. M., Hovenier, J. W., & Waters, B. F. M. 2004, A&A, 428, 663
Vanderbei, R. J., Kasdin, N. J., & Spergel, D. N. 2004, ApJ, 615, 555
Wuchterl, G. 2000, in ESO Astrophysics Symp., From Extrasolar Planets to Cosmology: The VLT Opening Symposium, ed. J. Bergeron, & A. Renzini (New York: Springer-Verlag), 408
Zubko, N., et al. 2007, Opt. Express, 15, 12189